Current Opinion in Colloid & Interface Science 18 (2013) 524–531

Contents lists available at ScienceDirect

Current Opinion in Colloid & Interface Science

journal homepage: www.elsevier.com/locate/cocis

Extension of the ladder model of self-assembly from cylindrical to disclike surfactant micelles

Peter A. Kralchevsky [a,*], Krassimir D. Danov [a], Svetoslav E. Anachkov [a], Gergana S. Georgieva [a], Kavssery P. Ananthapadmanabhan [b]

[a] Department of Chemical Engineering, Faculty of Chemistry and Pharmacy, Sofia University, Sofia 1164, Bulgaria
[b] Unilever Research & Development, 40 Merritt Blvd., Trumbull, CT 06611, USA

ARTICLE INFO

Article history:
Received 23 August 2013
Received in revised form 7 October 2013
Accepted 2 November 2013
Available online 7 November 2013

Keywords:
Disclike micelles
Nanodiscs
Cylindrical micelles
Self-assembly
Radius of gyration
Hydrodynamic radius

ABSTRACT

The ladder model of growth of cylindrical micelles gives expressions for the micellar size distribution and for the mean aggregation number, which are in good agreement with the experiment. Here, we consider this model and its extension to the case of disclike micelles. In analogy with the modeling of elongated micelles as spherocylinders, the disclike micelles can be modeled as toro-discs. Upon micelle growth, the hemispherical caps of a cylindrical aggregate remain unchanged, whereas the semitoroidal periphery of a disclike micelle expands. This effect can be taken into account in the expression for the size distribution of the disclike micelles, which predicts the dependence of the micelle mean aggregation number on the surfactant concentration. It turns out that disclike micelles could form in a limited range of surfactant concentrations, and that their mean aggregation number cannot exceed a certain maximal value. Large disclike micelles can exist only near the border with the domain of cylindrical micelles. Then, small variations in the experimental conditions could induce a transformation of the disclike micelles into cylindrical ones.

1. Introduction

The disclike surfactant micelles can be considered as predecessors of the lamellar phase in the same way as the cylindrical micelles are predecessors of the formation of hexagonal phase. Then, a question arises: Why do the disclike micelles represent a rare form of self-assembly [1,2], despite the fact that lamellar phases are often observed? In the present article, we will try to answer this question on the basis of a recently developed model of the growth of disclike micelles [3], which upgrades the ladder model for cylindrical micelles [4].

Although disclike micelles are not so frequently observed, there is a considerable amount of accumulated experimental material from the investigations of such self-assemblies, termed also nanodiscs or bicelles. Single component disclike micelles have been detected in solutions of anionic [5]; nonionic [6] and fluorinated surfactants [7–10]. Nanodiscs have been observed and investigated in various binary mixtures of cationic and anionic (catanionic) surfactant solutions [1,11–15]. Discoidal micelles and nematic phase from such micelles have been detected in ternary mixtures of lauric acid with anionic and zwitterionic surfactants [16]. Disc-shaped aggregates are formed also in solutions of diblock and triblock copolymers [17–22]. Such aggregates are formed also by phospholipids dispersed in water [23,24] and in aqueous surfactant/lipid systems [25]. The self-assembly of discoidal micelles has been found to be a transitional kinetic stage in the processes of formation and decomposition of liposomes [26,27]. Disc-shaped aggregates have been discovered also in solutions of bile salts [28–30] and their mixtures with phospholipids [31].

Shape polydispersity and shape fluctuations in ionic surfactant micelles have been analyzed and transitions from spherical micelles to prolate and oblate spheroids have been predicted in the frame of a theoretical model [32] as well as by computer simulations [33]. Branching instabilities in growing cylindrical and disclike micelles have been also investigated [34]. The formation of such micelles and their transformation into liquid crystalline phases was theoretically described in terms of the Helfrich's curvature moduli [35,36] and lattice Hamiltonian models [37]. The phase transitions between isotropic and columnar phases (for rodlike micelles), as well as between isotropic and lamellar phases (for disclike micelles) have been theoretically studied [38]. It was established that the size of the cylindrical aggregates increases continuously with concentration, while the size of the discs could jump from small to infinite [37,39]. For cylindrical micelles, there are molecular–thermodynamic models, coupled with geometrical-constraint considerations, which quantitatively predict the micelle growth with the rise of surfactant concentration [4,40,41]. A molecular–thermodynamic model of disclike micelles was recently developed [3], which quantitatively describes the variation in the micelle size with the increase of surfactant concentration in agreement with the experiment.

To answer the question formulated in the beginning, here we first compare expressions for the mean aggregation number and area per surfactant-molecule headgroup for different micellar geometries:

* Corresponding author. Fax: +359 2 9625643.
E-mail address: pk@lcpe.uni-sofia.bg (P.A. Kralchevsky).

1359-0294/$ – see front matter © 2013 Elsevier Ltd. All rights reserved.
http://dx.doi.org/10.1016/j.cocis.2013.11.002

spherical, cylindrical, discoidal and toroidal (Section 2). Next, the ladder model for cylindrical micelles is considered (Section 3) in view of its subsequent generalization to disclike micelles (Section 4). Special attention is paid to the size distribution of the disclike micelles; to its application for predicting the micelle mean aggregation number and to the limitations on the growth of such micelles.

2. Geometrical relations for spherical, cylindrical and disclike micelles

2.1. Aggregation number and area per molecule

Because of the different surface curvature of spherical, cylindrical and disclike micelles, the surface area per headgroup is the largest for the spherical micelles and the smallest for the disclike ones. For the needs of the ladder model extension, here we summarize the basic equations that quantify this effect. For simplicity, we will consider single-component micelles. If the composition of mixed micelles is independent of their size (negligible segregation effects due to the greater peripheral curvature), the expressions for single-component micelles can be applied to multi-component ones in terms of average values [3].

For a *spherical micelle*, we have the following estimates [40,41]:

$$n_s = \frac{\frac{4}{3}\pi R^3}{v}, \qquad a_s = \frac{4\pi R^2}{n_s} = \frac{3v}{R} \tag{2.1}$$

n_s is the aggregation number of the spherical micelle; R is the radius of its hydrophobic core; a_s is the area per molecule relative to the surface of the hydrophobic core; v is the volume per hydrocarbon chain in the micelle.

Assuming that a *cylindrical micelle* consists of a cylinder of length L and two hemispherical caps of radius R equal to the cylinder's radius (Fig. 1), we obtain:

$$n_c = \frac{\pi R^2 L}{v}, \qquad a_c = \frac{2\pi RL}{n_c} = \frac{2v}{R} \tag{2.2}$$

n_c is the aggregation number of the cylindrical part of the micelle; a_c is the area per molecule relative to the cylindrical part of the surface of the hydrophobic core.

In analogy with the cylindrical micelles, which are modeled as "sphero-cylinders", the disclike micelles can be modeled as "toro-discs", consisting of a disc of diameter L and thickness $2R$, and of a periphery that represents a semitorus of radius R (Fig. 1). The volume and the surface area of the disclike micelle can be expressed in the form:

$$V = V_d + V_t, \qquad A = A_d + A_t \tag{2.3}$$

where the indices 'd' and 't' refer to the discoidal and toroidal parts of the micelle, respectively. The volume and the surface area of the discoidal part are:

$$V_d = \frac{\pi}{2} RL^2, \qquad A_d = \frac{\pi}{2} L^2 \tag{2.4}$$

Likewise, the volume and surface area of the toroidal periphery of the micelle are [3]:

$$V_t = \frac{\pi^2}{2} R^2 L + \frac{4}{3}\pi R^3, \qquad A_t = \pi^2 RL + 4\pi R^2. \tag{2.5}$$

The number of surfactant molecules n_d and the area a_d in the *discoidal part* of the micelle are as follows:

$$n_d = \frac{V_d}{v} = \frac{\pi RL^2}{2v}, \qquad a_d = \frac{\pi L^2}{2n_d} = \frac{v}{R} \tag{2.6}$$

where Eq. (2.4) was used. Summarizing Eqs. (2.1), (2.2) and (2.6), we obtain:

$$a_d = \frac{v}{R}, \qquad a_c = \frac{2v}{R}, \qquad a_s = \frac{3v}{R}. \tag{2.7}$$

In other words, the area per molecule is the smallest for the discoidal part of a micelle and the largest for a spherical micelle.

For the *toroidal periphery* of the disclike micelle, in analogy with Eq. (2.6), using Eq. (2.5) we obtain:

$$n_t = \frac{V_t}{v} = \frac{1}{v}\left(\frac{\pi^2}{2} R^2 L + \frac{4}{3}\pi R^3\right), \tag{2.8}$$

$$a_t = \frac{A_t}{n_t} = \frac{\pi L + 4R}{\pi L + \frac{8}{3}R} \frac{2v}{R} \tag{2.9}$$

where n_t and a_t are, respectively, the total number of surfactant molecules and the area per molecule in the toroidal part of the disclike micelle. Eq. (2.8) shows how the number of surfactant molecules in the toroidal part of the micelle increases with the micelle diameter L. In the limit $L = 0$, the "toro-disc" becomes a sphere, and Eq. (2.8) yields $n_t = n_s$; see Eq. (2.1).

The comparison of Eqs. (2.1), (2.2) and (2.9) leads to the following inequalities:

$$\frac{2v}{R} = a_c \le a_t \le a_s = \frac{3v}{R}. \tag{2.10}$$

Thus, the area per molecule in the toroidal part of the micelle is greater than that for a cylindrical micelle, but smaller than that for a spherical micelle. For large disclike micelles ($L \to \infty$), Eq. (2.9) yields $a_t \to a_c$, whereas for small disclike micelles ($L \to 0$), Eq. (2.9) yields $a_t \to a_s$.

The expression $a_d = v/R$ was obtained only on the basis of considerations about the radius and volume of the micelle *hydrophobic core*; see Eq. (2.6). This is possible only if the surfactant headgroups are relatively small and do not impose any geometrical constraints. For the *headgroups*, we can define a_h as the average excluded area per headgroup at close packing, projected on the surface of the micelle

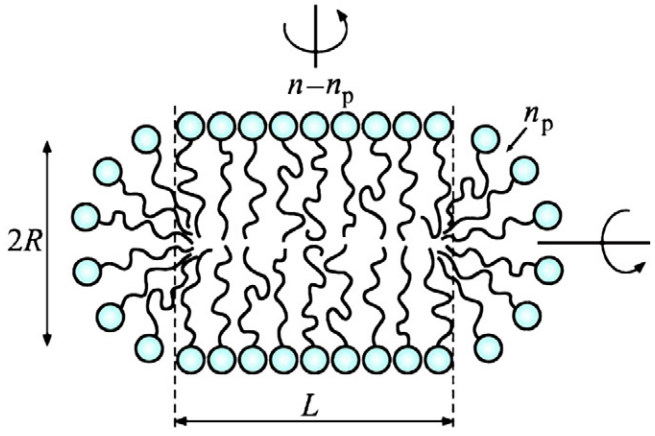

Fig. 1. Sketch of a micelle of aggregation number n, which includes n_p molecules belonging to the micellar periphery. A rotation around the *horizontal* axis yields a sphero-cylindrical micelle of cylinder length L and radius R, which equals the radius of the two hemispherical caps. A rotation around the *vertical* axis yields a toro-disc shaped micelle with disc diameter L and thickness $2R$, where R is also the radius of the micelle semitoroidal periphery.

hydrophobic core. Apparently, we should have $a_d \geq a_h$. Then, the generalized definition of a_d is [3]:

$$a_d = \begin{cases} v/R & \text{for } v/R > a_h \\ a_h & \text{for } v/R \leq a_h \end{cases}. \tag{2.11}$$

2.2. Radius of gyration and hydrodynamic radius

By static and dynamic light scattering one can determine the micelle mean *radius of gyration*, R_g, and *hydrodynamic radius*, R_h [42–44]. Next, if the micelle is modeled as a prolate or oblate spheroid, from the measured R_g, and R_h one can calculate the mean values of the spheroid semi-major and semi-minor axes, a and b [45].

For disclike micelles, the toro-disc model is more realistic than the one with oblate spheroid. For toro-disc shaped micelles, the following expressions for R_g, and R_h have been recently derived [3]:

$$R_g^2 = \frac{L^2}{8}\frac{1 + 2\pi u + 56u^2/3 + 8\pi u^3 + 64u^4/5}{1 + \pi u + 8u^2/3}, \tag{2.12}$$

$$R_h = b + \frac{3}{8}L, \qquad (\text{toro}-\text{disc}) \tag{2.13}$$

where $u = b/L$; by definition, $b = R + \delta_h$ is the length of the surfactant molecule, where R is the length of the surfactant hydrophobic chain and δ_h, is the surfactant headgroup diameter.

Eqs. (2.12) and (2.13) can be used as a *criterion* to prove whether the micelles are *disclike* from experimental light scattering data for R_h and R_g. The parameter b is usually known — it is approximately equal to the length of the surfactant molecule, estimated from molecular-size considerations [41]. Then, from Eq. (2.13) we find $L = 8(R_h - b)/3$. Next, L is substituted in Eq. (2.12) to calculate R_g. If the calculated and measured R_g values are close, then the micelles should be disclike.

A similar criterion for *cylindrical* (rodlike) micelles can be based on analogous theoretical expressions for R_h and R_g, as follows [45]:

$$R_h = \frac{b\exp(s)}{2s - 0.19 - \dfrac{8.24}{s} + \dfrac{12}{s^2}}, \tag{2.14}$$

$$R_g = \left(\frac{L^2}{12} + \frac{b^2}{2}\right)^{1/2} \qquad (\text{hard rod}) \tag{2.15}$$

where $s = \ln(L/b)$; L and b are, respectively, the cylinder's length and radius.

It should be noted that Eqs. (2.14) and (2.15) are derived for cylinders *without* hemispherical caps. For sufficiently large micelles, the hemispherical caps give a negligible contribution to R_h and R_g, but make the respective integrals unsolvable in terms of elementary functions.

3. The ladder model for cylindrical micelles

3.1. Micelle size distribution

The ladder model by Missel et al. [4] was initially derived to describe the growth of cylindrical micelles. It is based on the chemical equilibrium relationship between the micelles of aggregation number n and the free surfactant monomers:

$$n\mu_1 = \mu_n \tag{3.1}$$

where $\mu_1 = \bar{\mu}_1 + kT\ln X_1$ and $\mu_n = \bar{\mu}_n + kT\ln X_n$ are the chemical potentials of the monomers and micelles, respectively; $\bar{\mu}_1$ and $\bar{\mu}_n$ are standard chemical potentials; X_1 and X_n are the molar fractions of monomers and micelles of aggregation number n in the solution; k is the Boltzmann constant; T is the absolute temperature. Substituting the latter expressions in Eq. (3.1) and taking inverse logarithm, we obtain the micelle size distribution [4]:

$$X_n = X_1^n \exp\left(-\frac{\bar{\mu}_n - n\bar{\mu}_1}{kT}\right). \tag{3.2}$$

So far, we did not make any assumptions concerning the micelle shape. Hence, Eq. (3.2) is applicable to both cylindrical and disclike micelles. Generalization to multi-component micelles can be found in Ref. [3].

The basic assumption of the ladder model is that the standard chemical potential of the cylindrical micelle is a sum of contributions from its cylindrical part and from its two hemispherical caps [4]:

$$\bar{\mu}_n = \bar{\mu}^{(c)}(n - n_s) + \bar{\mu}^{(s)}n_s. \tag{3.3}$$

This relationship corresponds to Fig. 1 with $n_p = n_s$; $\bar{\mu}^{(s)}$ and $\bar{\mu}^{(c)}$ are the standard chemical potentials of surfactant molecules in the *spherical* and *cylindrical* parts of the micelle, respectively; n is the total number of surfactant molecules contained in the micelle, whereas n_s is the total number of surfactant molecules contained in the two hemispherical caps. Substituting Eq. (3.3) into Eq. (3.2), one obtains [4]:

$$X_n = \frac{1}{K}\left(\frac{X_1}{X_B}\right)^n, \quad \frac{X_1}{X_B} < 1, \quad n \geq n_s \tag{3.4}$$

where

$$K = \exp\left(\frac{n_s\left(\bar{\mu}^{(s)} - \bar{\mu}^{(c)}\right)}{kT}\right), \tag{3.5}$$

$$X_B = \exp\left(\frac{\bar{\mu}^{(c)} - \bar{\mu}_1}{kT}\right). \tag{3.6}$$

Eq. (3.4) represents the micelle size-distribution for $n \geq n_s$, where $n = n_s$ corresponds to the smallest spherical micelles. Eq. (3.4) implies that the micelle concentration X_n exponentially decreases with the rise of the aggregation number n. The total (input) molar fraction of surfactant in the solution is:

$$X = X_1 + \sum_{n=n_s}^{\infty} nX_n \tag{3.7}$$

The substitution of Eq. (3.4) into Eq. (3.7) yields:

$$K(X - X_1) = \sum_{n=n_s}^{\infty} nq^n = \sum_{n=n_s}^{\infty}\left[n_s q^n + (n - n_s)q^n\right] \tag{3.8}$$

where $q \equiv X_1/X_B$ must be smaller than 1 to have a convergent series. The first term in the brackets expresses the contribution from the hemispherical caps, whereas the second term is the contribution from the micelle cylindrical part (Fig. 1). The summation in Eq. (3.8) leads to:

$$K(X - X_1) = (1 - \varepsilon)^{n_s}\left[\frac{n_s}{\varepsilon} + \frac{1 - \varepsilon}{\varepsilon^2}\right] \tag{3.9}$$

where $\varepsilon = 1 - q$. As above, the two terms in the brackets in Eq. (3.9) represent, respectively, contributions from the hemispherical caps and from the cylindrical parts of the micelles. If large cylindrical (rodlike or wormlike) micelles are present in the solution, then the last term in the brackets must be predominant, which means that the growth of micelles with the rise of surfactant concentration corresponds to $\varepsilon \to 0$.

3.2. Mass-average micelle aggregation number

By definition the mass-average micelle aggregation number is:

$$\overline{n}_M = \left(\sum_{n=n_s}^{\infty} n^2 X_n\right) \Big/ \sum_{n=n_s}^{\infty} n X_n. \tag{3.10}$$

In view of Eqs. (3.4), (3.7) and (3.9), the summation in Eq. (3.10) yields [4]:

$$\overline{n}_M = \frac{2}{\varepsilon} - 1 + \frac{n_s(n_s-1)\varepsilon}{1+(n_s-1)\varepsilon} \quad \text{(cylindrical micelles)} \tag{3.11}$$

Eqs. (3.9) and (3.11) give the dependence of $\overline{n}_M$ on the total surfactant concentration, X, in a parametric form: $X = X(\varepsilon)$ and $\overline{n}_M = \overline{n}_M(\varepsilon)$. An approximate asymptotic expression for the dependence $\overline{n}_M(X)$ at large $K(X - X_1)$ can be obtained by expanding in series in Eqs. (3.9) and (3.11), and eliminating ε [3,4]:

$$\overline{n}_M = 2[K(X-X_1)]^{1/2} + \frac{1+6n_s(n_s-1)}{4[K(X-X_1)]^{1/2}} + O\left(\frac{1}{K(X-X_1)}\right) \tag{3.12}$$

The first term in the right-hand side is the leading one, so that the plot of $\overline{n}_M$ vs. $(X - X_1)^{1/2}$ must be a straight line with slope $2\,K^{1/2}$ [4].

Fig. 2 shows a plot of data for $\overline{n}_M$ vs. $(X - X_1)^{1/2}$ from Ref. [46] for cylindrical micelles formed in aqueous solutions of the anionic surfactant sodium lauryl ether sulfate with two ethylene-oxide groups (SLES-2EO). All solutions contain 0.7 M NaCl, which suppresses the electrostatic repulsion between the surfactant headgroups and promotes the micelle growth. As seen in Fig. 2, the experimental data comply well with a straight line in agreement with Eq. (3.12). The slope of the straight line is $K = 5.22 \times 10^9$, which confirms that the quantity $K(X - X_1)$, used in the power expansion, Eq. (3.12), is really large in the experimental range of X values.

4. The ladder model for disclike micelles

4.1. Size distribution of the disclike micelles

The disclike micelle can be modeled as a combination of disc and torus (toro-disc, see Fig. 1). Then, the micelle standard chemical potential $\widetilde{\mu}_n$ can be expressed in the form:

$$\overline{\mu}_n = \overline{\mu}^{(d)}(n - n_t) + \overline{\mu}^{(t)} n_t \tag{4.1}$$

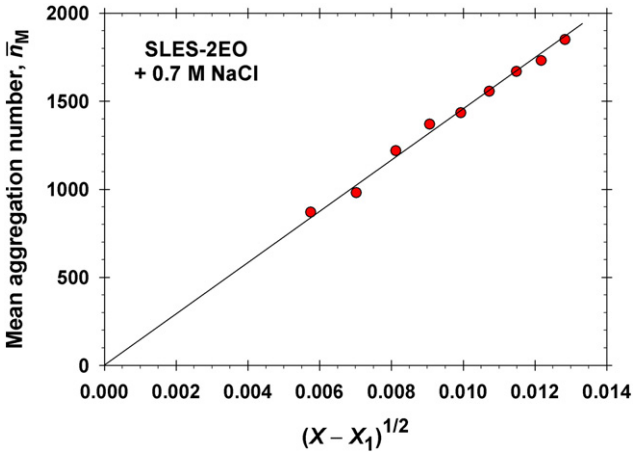

Fig. 2. Plot of the mass-average aggregation number, $\overline{n}_M$, of cylindrical micelles vs. $(X - X_1)^{1/2}$ for solutions of SLES-2EO containing 0.7 M NaCl; data from Ref. [46]. The monomer mole fraction X_1 corresponds to the CMC.

As before, n is the total aggregation number; n_t is the number of surfactant molecules in the semitoroidal periphery of the micelle; $\overline{\mu}^{(d)}$ and $\overline{\mu}^{(t)}$ are standard chemical potentials of a molecule that belongs, respectively, to the discoidal and toroidal part of the micelle. For disclike micelles, n_t and the area per molecule in the toroidal periphery, a_t, depend on L; see Eqs. (2.8) and (2.9). For this reason, $\overline{\mu}^{(t)}$ also depends on L. To take into account this dependence, in Eq. (4.1) we can expand $\overline{\mu}^{(t)}$ in series around $a = a_s$ [3]:

$$\begin{aligned}\overline{\mu}_n &= \overline{\mu}^{(d)} n + \left(\overline{\mu}^{(t)} - \overline{\mu}^{(d)}\right) n_t \\ &\approx \overline{\mu}^{(d)} n + \left[\overline{\mu}^{(s)} + \frac{\partial \overline{\mu}}{\partial a}\Big|_{a=a_s} (a_t - a_s) - \overline{\mu}^{(d)}\right] n_t.\end{aligned} \tag{4.2}$$

Using Eqs. (2.8) and (2.9), after some transformations described in Ref. [3], one obtains:

$$\overline{\mu}_n - n\overline{\mu}^{(1)} \approx \left(\overline{\mu}^{(s)} - \overline{\mu}^{(d)}\right) n_s + \left(\overline{\mu}^{(d)} - \overline{\mu}^{(1)}\right) n + \left(\overline{\mu}^{(c)} - \overline{\mu}^{(d)}\right) \frac{3\pi L}{8R}\, n_s. \tag{4.3}$$

The substitution of Eq. (4.3) in Eq. (3.2) leads to the following expression for the size distribution of the disclike micelles [3]:

$$X_n = \frac{1}{K} \exp\left(-\varepsilon n - \frac{3\pi}{8} n_s p x\right) \tag{4.4}$$

where

$$K \equiv \exp\left(\frac{\overline{\mu}^{(s)} - \overline{\mu}^{(d)}}{kT} n_s\right), \tag{4.5}$$

$$X_B \equiv \exp\left(\frac{\overline{\mu}^{(d)} - \overline{\mu}^{(1)}}{kT}\right), \tag{4.6}$$

$$x = \frac{L}{R}, \quad \frac{\overline{X}_1}{\overline{X}_B} = \exp(-\varepsilon), \tag{4.7}$$

$$p = \frac{\overline{\mu}^{(c)} - \overline{\mu}^{(d)}}{kT} \tag{4.8}$$

For $p = 0$, Eq. (4.4) is mathematically identical to the respective expression for cylindrical micelles, Eq. (3.4). The term with p in Eq. (4.4) accounts for the increment of the excess peripheral energy of the disclike micelle. For positive p, the peripheral energy increases with the rise of disc diameter. The quantities n and x are not independent. Combining Eqs. (2.1), (2.6), (2.8) and (4.7), we obtain:

$$n = n_d + n_t = \frac{3n_s}{8} x^2 + \frac{3n_s}{8} \pi x + n_s. \tag{4.9}$$

It is convenient to represent the micelle size distribution, Eq. (4.4), in the form:

$$X_n = \frac{1}{K} \exp\left[-\varepsilon_s x^2 - \pi(p_s + \varepsilon_s)x - \frac{8}{3}\varepsilon_s\right] \tag{4.10}$$

where

$$\varepsilon_s \equiv \frac{3n_s}{8}\varepsilon \quad \text{and} \quad p_s \equiv \frac{3n_s}{8} p. \tag{4.11}$$

4.2. Total surfactant molar fraction and mass-average aggregation number

The total surfactant molar fraction X is given by Eq. (3.7). In view of Eq. (4.10), it is convenient to replace the summation by integration using the Euler–Maclaurin formula:

$$X-X_1=\sum_{n=n_s}^{\infty} nX_n \approx \frac{n_s X_{n_s}}{2}+\int_{n_s}^{\infty} nX_n dn. \tag{4.12}$$

Substituting n and X_n from Eqs. (4.9) and (4.10) in Eq. (4.12), and solving the integral, we obtain [3]:

$$K(X-X_1)=\left(\frac{3n_s}{8}\right)^2 \exp\left(-\frac{8\varepsilon_s}{3}\right)\left(\frac{32}{9n_s}+J_1\right) \tag{4.13}$$

where

$$J_1=\frac{3\pi^2 p_s(p_s-\varepsilon_s)+4\varepsilon_s(3+8\varepsilon_s)}{12\varepsilon_s^3} -\frac{3\pi^2\left(p_s^2-\varepsilon_s^2\right)+2\varepsilon_s(9+16\varepsilon_s)}{24\varepsilon_s^{7/2}} p_s\pi^{3/2}(1-erf\xi)e^{\xi^2}. \tag{4.14}$$

erfξ is the conventional error function, and

$$\xi \equiv \frac{\pi(p_s+\varepsilon_s)}{2\varepsilon_s^{1/2}} \tag{4.15}$$

The mass-average aggregation number $\overline{n}_M$ is defined by Eq. (3.10), where the summation can be replaced by integration, as in Eq. (4.12). In this way, using Eq. (4.10), one derives [3]:

$$\overline{n}_M=\frac{3n_s}{8}\left(\frac{256}{27n_s}+J_2\right)\Big/\left(\frac{32}{9n_s}+J_1\right) \tag{4.16}$$

where J_1 is given by Eqs. (4.14) and

$$J_2=\frac{1}{144\varepsilon_s^5}\left[9\pi^4 p_s^3(p_s-\varepsilon_s)+162\pi^2 p_s^2\varepsilon_s+3\pi^2\left(64-3\pi^2\right)p_s^2\varepsilon_s^2 -126\pi^2 p_s\varepsilon_s^2-3\pi^2\left(64-3\pi^2\right)p_s\varepsilon_s^3+32\varepsilon_s^2\left(9+24\varepsilon_s+32\varepsilon_s^2\right)\right] -\frac{p_s\pi^{3/2}}{288\varepsilon_s^{11/2}}\left[9\pi^4 p_s^4+180\pi^2 p_s^2\varepsilon_s+6\pi^2\left(32-3\pi^2\right)p_s^2\varepsilon_s^2 +540\varepsilon_s^2+36\left(32-3\pi^2\right)\varepsilon_s^3+\left(32-3\pi^2\right)^2\varepsilon_s^4\right](1-erf\xi)\exp\left(\xi^2\right) \tag{4.17}$$

Eqs. (4.13) and (4.16) determine the concentration dependence of the mass average aggregation number, $\overline{n}_M(X)$, in a parametric form, viz. $X=X(\varepsilon_s)$ and $\overline{n}_M=\overline{n}_M(\varepsilon_s)$.

4.3. Standard chemical potential of a surfactant molecule in the micelles

The series expansion in Eq. (4.2) implicitly assumes the existence of a universal dependence of the standard chemical potential of a surfactant molecule in a micelle on the area per headgroup: $\overline{\mu}=\overline{\mu}(a)$. The quantities $\overline{\mu}^{(d)}$, $\overline{\mu}^{(c)}$ and $\overline{\mu}^{(s)}$ in Eq. (4.3) can be defined as follows [3]:

$$\overline{\mu}^{(d)}\equiv\overline{\mu}(a_d),\quad \overline{\mu}^{(c)}\equiv\overline{\mu}(a_c),\quad \overline{\mu}^{(s)}\equiv\overline{\mu}(a_s) \tag{4.18}$$

where the areas per molecule in the discoidal, cylindrical and spherical parts of a micelle, a_d, a_c and a_s, are given by Eqs. (2.7) and (2.11).

At a given composition of the micelles, the dependence $\overline{\mu}=\overline{\mu}(a)$ is expected to have a minimum [41], as sketched in Fig. 3. At smaller a, the intermolecular repulsion prevails, whereas at larger a, the increased contact area between the micelle hydrophobic core with the surrounding water gives rise to an effective attraction.

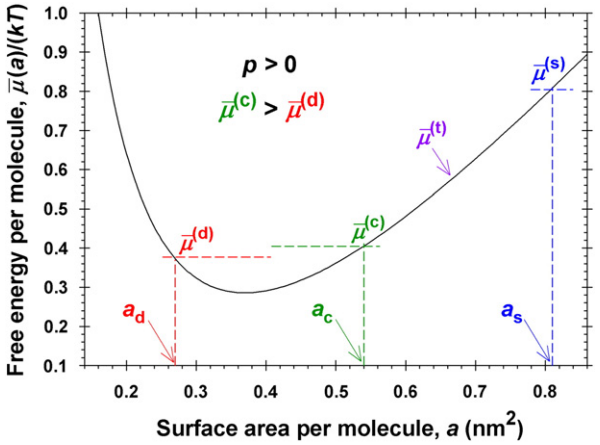

Fig. 3. Illustrative plot of the interaction free energy per surfactant molecule $\overline{\mu}$, scaled with kT, vs. the surface area per surfactant molecule in the micelle, a, for $p\equiv\left(\overline{\mu}^{(c)}-\overline{\mu}^{(d)}\right)/(kT)>0$, at which disclike micelles are formed; details in the text.

Based on estimates of the Gibbs free energy of the micellar solution, $G=\Sigma_i N_i\mu_i$, in Ref. [3] it is proven that if $p\equiv\left(\overline{\mu}^{(c)}-\overline{\mu}^{(d)}\right)/(kT)<0$, then the formation of *cylindrical* micelles is energetically favorable. In contrast, for $p>0$ *disclike* micelles should form.

Furthermore, the fits of experimental data for $\overline{n}_M$ vs. X for disclike micelles with the general model from Section 4.2 give values of p, which are positive, but close to zero [3]. In view of Eq. (4.18), this implies $\overline{\mu}(a_c)\approx\overline{\mu}(a_d)$. However, a_c is considerably greater than a_d; for example, we could have $a_c=2a_d$; see Eq. (2.7). In such a case, the relation $\overline{\mu}(a_c)\approx\overline{\mu}(a_d)$ can be fulfilled only if a_c and a_d are located on the two sides of the minimum of the function $\overline{\mu}(a)$, as sketched in Fig. 3.

What concerns the chemical potential of a monomer in the *toroidal periphery* of a disclike micelle, $\overline{\mu}^{(t)}\equiv\overline{\mu}(a_t)$, we have $\overline{\mu}^{(c)}\le\overline{\mu}^{(t)}\le\overline{\mu}^{(s)}$ insofar as $a_c\le a_t\le a_s$, see Eqs. (2.10), (4.18) and Fig. 3. For this reason, it was possible to estimate the derivative in Eq. (4.2) by using linear interpolation: $\partial\overline{\mu}/\partial a=\left(\overline{\mu}^{(s)}-\overline{\mu}^{(c)}\right)/(a_s-a_c)$.

4.4. Limitations on the growth of disclike micelles

As mentioned above, at $p<0$ the formation of disclike micelles is energetically disadvantageous, and therefore cylindrical micelles are formed in that case. Here, we will focus on the opposite case, $p>0$, which corresponds to $\overline{\mu}^{(d)}<\overline{\mu}^{(c)}$ (Fig. 3) and to the formation of *disclike* micelles. At positive p, the quantities J_1 and J_2 in Eqs. (4.14) and (4.17) are finite for $\varepsilon_s\to 0$. The maximal values of J_1 and J_2, which are attained at $\varepsilon_s=0$, are:

$$J_{1,\max}=\frac{12}{\pi^4 p_s^4}+\frac{6}{\pi^2 p_s^3}+\frac{16+3\pi^2}{3\pi^2 p_s^2}+\frac{8}{3p_s} \tag{4.19}$$

$$J_{2,\max}=\frac{240}{\pi^6 p_s^6}+\frac{120}{\pi^4 p_s^5}+\frac{64+24\pi^2}{\pi^4 p_s^4}+\frac{32+2\pi^2}{\pi^2 p_s^3}+\frac{128+48\pi^2}{9\pi^2 p_s^2}+\frac{64}{9p_s}. \tag{4.20}$$

Setting $\varepsilon_s\to 0$ in Eq. (4.13), we obtain the maximum value of X, denoted X_{max}:

$$X_{\max}=X_1+\frac{1}{K}\left(\frac{3n_s}{8}\right)^2\left(\frac{32}{9n_s}+J_{1,\max}\right) \tag{4.21}$$

where $J_{1,max}$ is given by Eq. (4.19). From a physical viewpoint, this result means that for $p>0$, disclike micelles can be formed only in a *limited*

range of surfactant concentrations, viz. $X_1 < X \le X_{max}$. For a given p (for a given system), at $X = X_{max}$, the micelle mass-average aggregation number $\overline{n}_M$ attains its maximal value, $\overline{n}_{M,max}$. It can be calculated by replacing J_1 and J_2 in Eq. (4.16) with their maximal values given by Eqs. (4.19) and (4.20).

To illustrate the dependence of X_{max} on p, in Fig. 4a we have plotted $X_{max} - X_1$ vs. p calculated from Eq. (4.21) at experimental parameter values, $n_s = 83$ and $\ln K = 35.2$ (see Fig. 4c and Section 4.5). The plot indicates that disclike micelles could exist only in the region confined between the two axes of the coordinate system and the theoretical curve $X_{max} - X_1$ vs. p. In this region, at small p and large X the surfactant can form a relatively concentrated dispersion of large disclike micelles, so that eventually nematic or smectic phases from such micelles could appear [7,16,47]. In the region $p < 0$ cylindrical micelles are formed (see above).

At $X > X_{max}$ (Fig. 4a) the formation of large lamellas is expected [1,47]. Indeed, at $p > 0$ the lower chemical potential of a molecule in the discoidal part of a micelle, $\overline{\mu}^{(d)} < \overline{\mu}^{(c)}$, favors the growth of *lamellar* structures. A theoretical analysis based on Ising Hamiltonians has also predicted that the size of disclike aggregates should jump from small to infinite [37,39]. In Fig. 4a, this should happen when crossing the boundary line $X_{max} - X_1$ vs. p.

Fig. 4b shows a plot of $\overline{n}_{M,max}$ vs. p at experimental parameter values [3] denoted in the figure. (Note that this plot is independent of K.) One sees that large disclike aggregates (with $\overline{n}_M > 10n_s$) could form only at $p < 0.01$. At $p < 3 \times 10^{-4}$, $\overline{n}_M$ could exceed 10^6. In contrast, at $p > 0.1$ we have $\overline{n}_{M,max} \approx n_s$, i.e. the disclike micelles are transformed into spherical ones. The limited range of p values, $0 < p < 0.1$, where disclike micelles can form (Fig. 4b) explains why they represent a rare form of self-assembly as compared to the cylindrical micelles.

For $0 < p < 0.01$, from Eq. (4.16) and (4.21), along with Eqs. (4.19) and (4.20), it follows that the leading terms of the series expansions of the respective quantities at $p << 1$ are [3]:

$$X_{max} - X_1 \approx \frac{256}{3\pi^4 K n_s^2}\frac{1}{p^4}; \qquad \overline{n}_{M,max} \approx \frac{160}{3\pi^2 n_s}\frac{1}{p^2} \tag{4.22}$$

The limitations on the growth of disclike micelles, related to the existence of maximal values, such as X_{max} and $\overline{n}_{M,max}$ calls for discussion. These maximal values appear because at $p > 0$ the infinite sums in Eqs. (3.10) and (4.12) are convergent for $\varepsilon \to 0$. (In contrast, for $p \le 0$ all these infinite sums diverge at $\varepsilon \to 0$, which corresponds to the growth of increasingly large micelles with the rise of surfactant concentration.) The convergence of the series at $p > 0$ is due to the term with p in Eq. (4.4), which takes into account the increment of the excess peripheral energy of the disclike micelle. Thus, disclike micelles could grow only at $p > 0$, but the positive p leads to a rise of the micelle peripheral energy, which in turns limits the micelle growth (Fig. 4a,b).

4.5. Interpretation of experimental data for disclike micelles

Because the values of p for disclike micelles are rather small (Fig. 4b), the procedure for determining p from experimental data is nontrivial. This procedure is illustrated in Fig. 4c with data from Ref. [3] for disclike micelles in solutions containing cocamidopropyl betaine (CAPB), sodium lauryl ether sulfate with one ethylene-oxide group (SLES) and lauric acid (LA). The experimental points correspond to various total surfactant concentrations, c_t, at the same molar ratio, 8:2:1, of the three components. The working solutions were obtained by dilution with water containing 110 mM NaCl, so that their ionic strength is fixed and the electrostatic interactions between the micelles are suppressed.

Experimental data for the micelle hydrodynamic radius, R_h, determined by dynamic light scattering are shown in Table 1. The mass-average aggregation number $\overline{n}_M$ is estimated by division of the total volume of the micelle hydrophobic core, V_{core}, on the mean volume per hydrocarbon tail, $\overline{v}$ [3]:

$$\overline{n}_M = \frac{V_{core}}{\overline{v}} \tag{4.23}$$

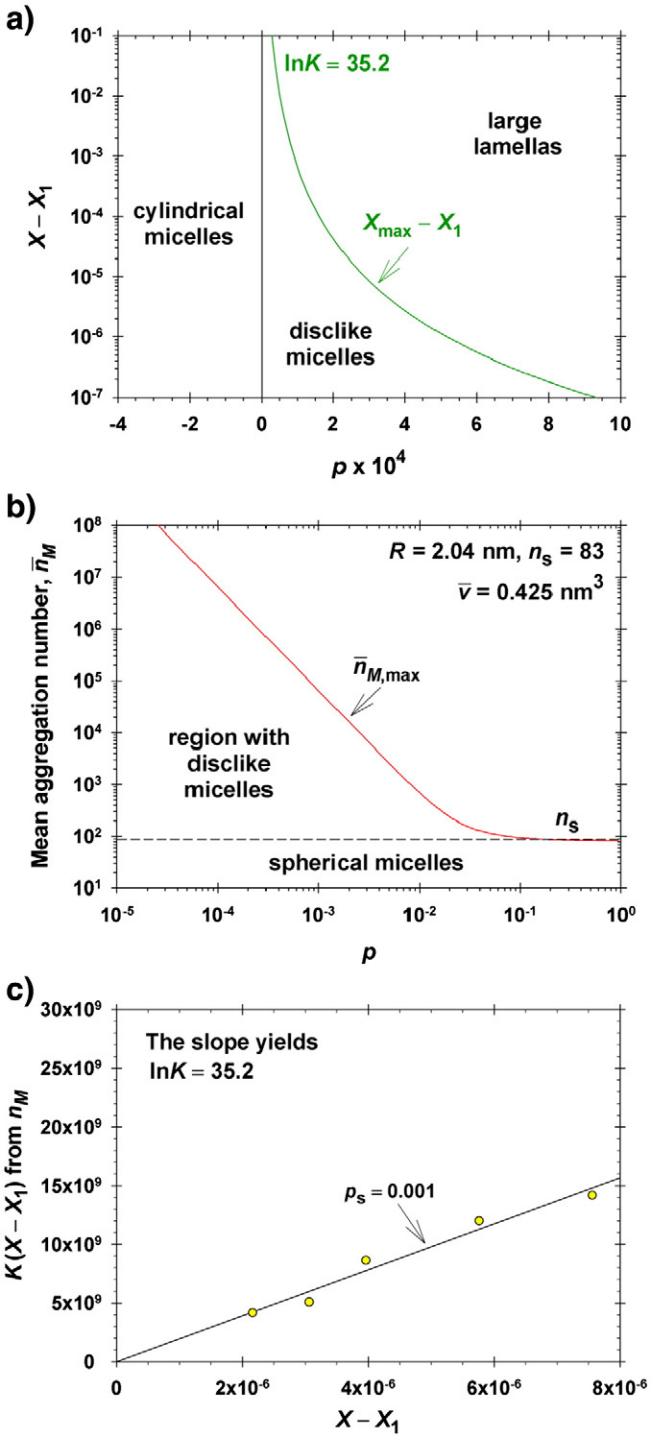

Fig. 4. (a) Plot of $X_{max} - X_1$ vs. p calculated from Eq. (4.21); the phase domains with different micelles are shown. (b) Plot of $\overline{n}_M$ vs. p calculated from Eqs. (4.16), (4.19) and (4.20). (c) Plot of data from Table 1 as $K(X - X_1)$ vs. $X - X_1$, where $K(X - X_1)$ is calculated from the experimental $\overline{n}_M$ using Eqs. (4.13) and (4.16), whereas $X - X_1$ is determined from c_t. The best fit is a straight line of zero intercept, which corresponds to $p_s = 0.001$ and $\ln K = 35.2$.

Table 1
Geometrical parameters of disclike micelles and their mean aggregation number $\overline{n}_M$ calculated by using the toro-disc model.

Experiment		Toro-disc		
c_t (mM)	R_h (nm)	$L/2 + b$ (nm)	V_{core} (nm^3)	$\overline{n}_M$, Eq. (4.23)
0.220	51.9	68.3	57,561	135,422
0.275	54.5	71.7	63,666	149,783
0.330	62.2	82.0	83,548	196,558
0.440	67.6	89.2	99,101	233,148
0.550	70.5	93.1	108,001	254,087

For determining V_{core}, the toro-disc model (Fig. 1) is applied:

$$V_{core} = V_d + V_t = \frac{\pi}{2}RL^2 + \frac{\pi^2}{2}R^2L + \frac{4}{3}\pi R^3 \tag{4.24}$$

where $L = 8(R_h - b)/3$, see Eqs. (2.4), (2.5) and (2.13), with $b = 2.8$ nm — the length of the CAPB molecule, and $R = 2.04$ nm. For each R_h, we calculated L, V_{core} and $\overline{n}_M$ using Eqs. (4.23) and (4.24); the results are given in Table 1.

Furthermore, the procedure for data processing and determining the parameters p and K is as follows [3]: (i) A tentative value is assigned to p_s. (ii) For each experimental value of $\overline{n}_M$ in Table 1, we calculate ε_s by solving numerically Eq. (4.16). (iii) The obtained ε_s is substituted in Eq. (4.13), and $K(X - X_1)$ is calculated using also Eqs. (4.14) and (4.15). (iv) The obtained $K(X - X_1)$ values, corresponding to different experimental $\overline{n}_M$, are plotted vs. the experimental $X - X_1$; see Fig. 4c.

The parameter p_s is varied until the plot of the calculated $K(X - X_1)$ vs. the experimental $X - X_1$ complies with a linear regression of zero intercept; see the solid line in Fig. 4c. This regression determines the physical value of p_s, and its slope gives the physical value of K. The points in Fig. 4c represent data from the first and last columns of Table 1, recalculated in terms of $(X - X_1)$ and $K(X - X_1)$ by using the above procedure. The best fit given by the solid line in Fig. 4c corresponds to $p_s = 0.001$ and $\ln K = 35.2$.

For $n_s = 83$, in view of Eq. (4.5) we calculate $\left(\overline{\mu}^{(s)} - \overline{\mu}^{(d)}\right)/(kT) = (\ln K)/n_s = 0.42$, which is a reasonable value. In addition, from Eqs. (4.8) and (4.11) we obtain $p = 3.2 \times 10^{-5}$. In spite of being small, the above value of p is accurately determined, because small variations in p_s produce a significant effect on the fit. Because the intercept of this plot is sensitive to X_1, the value of X_1 (i.e. the CMC) is essential for the present procedure of data processing, despite the relation $X_1 << X$.

At $p \to 0$, the size distribution of the disclike micelles, X_n, is gradually transformed into that for cylindrical micelles; compare Eqs. (3.4) and (4.4). In view of Eq. (3.10), the same is true also for $\overline{n}_M$. For this reason, at small p values the mass-average aggregation number of the disclike micelles $\overline{n}_M$ grows linearly with $(X - X_1)^{1/2}$, as predicted by Eq. (3.12). However, at not-too-small p values, which are observed for micelles from fluorinated surfactants [9], the plot of $\overline{n}_M$ vs. $(X - X_1)^{1/2}$ may deviate from straight line [3].

In Ref. [3], the existence of a "resonance peak" in viscosity is reported at a given ratio of the three components, viz. 80:20:12 CAPB/SLES/LA. This phenomenon consists in a jump of viscosity of the micellar solution from e.g. 10 to 600 mPa.s in the close vicinity of the aforementioned special composition of the ternary surfactant mixture. As a possible explanation, it was proposed that because p is expected to depend on the composition, this parameter could undergo a transition from small positive values (corresponding to disclike micelles) to negative values (corresponding to cylindrical micelles; see Fig. 4a) in the narrow concentration range where the peak of viscosity is observed. Such a transition should be accompanied with a large jump in the micelle aspect ratio that, in turns, would lead to the observed jump in solution's viscosity [48]; see Ref. [3] for details.

5. Conclusions

The above analysis allows us to answer the question asked in the beginning of this article, viz. if the disclike micelles are predecessors of the often observed lamellar phase, why they represent a rare form of self-assembly. The answer is that the same factor, which engenders the appearance of disclike micelles, simultaneously limits their growth. This factor is the difference between the chemical potentials of a surfactant molecule in a cylindrical and in a disclike micelle, which is characterized by the dimensionless parameter $p = \left(\overline{\mu}^{(c)} - \overline{\mu}^{(d)}\right)/kT$. Two basic quantities of micellar thermodynamics grow proportional to p: (i) the energy gain upon the formation of discoidal (instead of cylindrical) micelles and (ii) the increment of the peripheral energy of a disclike micelle. The outcome of the counteraction of these two opposing factors can be quantified through their effect on the micelle size distribution, Eq. (4.4). The results show that disclike micelles could form in a limited range of surfactant concentrations, $X_1 < X \le X_{max}$ (Fig. 4a), and that their mean aggregation number can vary in a limited domain (Fig. 4b).

Large disclike micelles can form only for small positive p values. However, in this case the micellar system is close to the border (at $p = 0$) between disclike ($p > 0$) and cylindrical ($p < 0$) micelles. Then, small variations in the experimental conditions (e.g. changes in temperature; variations in the composition of mixed micelles, or replacement of the common water with heavy water) could induce a transformation of the disclike micelles into cylindrical ones, or vice versa [3].

The positive excess peripheral energy of the disclike micelles preserves their round shape. Indeed, if a disclike micelle occasionally forms at $p < 0$, its peripheral energy would be negative, which would give rise to a branching instability [34]. Thus, it turns out that the same factor, which causes the appearance of disclike micelles and limits their growth, also stabilizes their shape.

Acknowledgments

The authors gratefully acknowledge the support from the National Science Fund of Bulgaria, Grant No. DID-02-18/2009; from Unilever Research & Development; from the FP7 project Beyond-Everest, and from the ESF COST Action CM1101.

References

[1] Zemb T, Dubios M, Deme B, Guli-Kryzywicki T. Self-assembly of flat nanodiscs in salt-free catanionic surfactant solutions. Science 1999;283:816–9.
[2] Song Y, Dorin RM, Garcia RM, Jiang Y-B, Wang H, Li P, Qiu Y, van Swol F, Miller JE, Shelnutt JA. Synthesis of platinum nanowheels using a bicellar template. J Am Chem Soc 2008;130:12602–3.
[3] Anachkov SE, Kralchevsky PA, Danov KD, Georgieva GS, Ananthapadmanabhan KP. Disclike vs. cylindrical micelles: generalized model of micelle growth and data interpretation. J Colloid Interface Sci 2014. http://dx.doi.org/10.1016/j.jcis.2013.11.002.
[4] Missel PJ, Mazer NA, Benedek GB, Young CY, Carey MC. Thermodynamic analysis of the growth of sodium dodecyl sulfate micelles. J Phys Chem 1980;84:1044–57.
[5] Rades T, Müller-Goymann CC. Investigations on the micellisation behaviour of fenoprofen sodium. Int J Pharm 1997;159:215–22.
[6] Danino D. Cryo-TEM of soft molecular assemblies. Curr Opin Colloid Interface Sci 2012;17:316–29.
[7] Holmes MC, Reynolds DJ, Boden N. Concentration–temperature dependence of the size and shape of the micelles in the cesium pentadecafluorooctanoate/water system. J Phys Chem 1987;91:5257–62.
[8] Iijima H, Kato T, Yoshida H, Imai M. Small-angle X-ray and neutron scattering from dilute solutions of cesium perfluorooctanoate. Micellar growth along two dimensions. J Phys Chem B 1998;102:990–5.
[9] Matsuoka K, Yonekawa A, Ishii M, Honda C, Endo K, Moroi Y, Abe Y, Tamura T. Micellar size, shape and counterion binding of N-(1,1-Dihydroperfluoroalkyl)-N, N, N-trimethylammonium chloride in aqueous solutions. Colloid Polym Sci 2006;285:323–30.
[10] Matsuoka K, Ishii M, Yonekawa A, Honda C, Endo K, Moroi Y, Abe Y, Tamura T. Aggregate structure of N-(perfluoroalkylmethyl)-N, N, N-trimethylammonium chloride by transmission electron microscopy. Bull Chem Soc Jpn 2007;80:1129–31.
[11] Eastoe J, Rogueda P, Shariatmadari D, Heenan R. Micelles of asymmetric chain catanionic surfactants. Colloids Surf A 1996;117:215–25.
[12] Jung H-T, Lee SY, Kaler EW, Coldren B, Zasadzinski JA. Gaussian curvature and the equilibrium among bilayer cylinders, spheres, and discs. PNAS 2002;99:15318–22.

[13] Hao J, Hoffmann H. Self-assembled structures in excess and salt-free catanionic surfactant solutions. Curr Opin Colloid Interface Sci 2004;9:279–93.
[14] Carrière D, Belloni L, Demé B, Dubois M, Vautrin C, Meister A, Zemb T. In-plane distribution in mixtures of cationic and anionic surfactants. Soft Matter 2009;5:4983–90.
[15] Blanco E, Olsson U, Ruso JM, Schulz PC, Prieto G, Sarmiento F. Phase behavior of semifluorinated catanionic mixtures: head group dependence and spontaneous formation of vesicles. J Colloid Interface Sci 2009;331:522–31.
[16] Colafemmina G, Recchia R, Ferrante AS, Amin S, Palazzo G. Lauric acid-induced formation of a lyotropic nematic phase of disk-shaped micelles. J Phys Chem B 2010;114:7250–60.
[17] Wu J, Pearce EM, Kwei TK, Lefebvre AA, Balsara NP. Micelle formation of a rod–coil diblock copolymer in a solvent selective for the rod block. Macromolecules 2002;35:1791–6.
[18] Edmonds WF, Li Z, Hillmyer MA, Lodge TP. Disk micelles from nonionic coil–coil diblock copolymers. Macromolecules 2006;39:4526–30.
[19] Cui H, Chen Z, Wooley KL, Pochan DJ. Controlling micellar structure of amphiphilic charged triblock copolymers in dilute solution via coassembly with organic counterions of different spacer lengths. Macromolecules 2006;39:6599–607.
[20] Cui H, Chen Z, Zhong S, Wooley KL, Pochan DJ. Block copolymer assembly via kinetic control. Science 2007;317:647–50.
[21] Yin L, Hillmyer MA. Disklike micelles in water from polyethylene-containing diblock copolymers. Macromolecules 2011;44:3021–8.
[22] Holder SJ, Sommerdijk NAJM. New micellar morphologies from amphiphilic block copolymers: disks, toroids and bicontinuous micelles. Polym Chem 2011;2:1018–28.
[23] Vinson PK, Bellare JR, Davis HT, Miller WG, Scriven LE. Direct imaging of surfactant micelles, vesicles, discs, and ripple phase structures by cryo-transmission electron microscopy. J Colloid Interface Sci 1991;42:74–91.
[24] Sanders CR, Landis GC. Reconstitution of membrane proteins into lipid-rich bilayered mixed micelles for NMR studies. Biochemistry 1995;34:4030–40.
[25] Johansson E, Sandström MC, Bergström M, Edwards K. On the formation of discoidal versus threadlike micelles in dilute aqueous surfactant/lipid systems. Langmuir 2008;24:1731–9.
[26] Leng J, Egelhaaf SU, Cates ME. Kinetic pathway of spontaneous vesicle formation. Europhys Lett 2002;59:311–7.
[27] Johnsson M, Edwards K. Liposomes, disks, and spherical micelles: Aggregate structure in mixtures of gel phase phosphatidylcholines and poly(ethylene glycol)-phospholipids. Biophys J 2003;85:3839–47.
[28] Kawamura H, Murata Y, Yamaguchi T, Igimi H, Tanaka M, Sugihara G, Kratohvil JP. Spin-label studies of bile salt micelles. J Phys Chem 1989;93:3321–6.
[29] Small DM. Size and structure of bile salt micelles: influence of structure, concentration, counterion concentration, pH, and temperature. Adv Chem Ser B 1968;84:31–52.
[30] Madenci D, Egelhaaf SU. Self-assembly in aqueous bile salt solutions. Curr Opin Colloid Interface Sci 2010;15:109–15.
[31] Mazer NA, Benedek GB, Carey MC. Quasielastic light-scattering studies of aqueous biliary lipid systems. Mixed micelle formation in bile salt–lecithin solutions. Biochemistry 1980;19:601–15.
[32] Halle B, Landgren M, Jönsson B. The shape of ionic micelles. J Phys Fr 1988;49:1235–59.
[33] Daful AG, Avalos JB, Mackie AD. Model shape transitions of micelles: spheres to cylinders and disks. Langmuir 2012;28:3730–43.
[34] Tang M, Carter WC. Branching mechanisms in surfactant micellar growth. J Phys Chem B 2013;117:2898–905.
[35] Kozlov MM, Lichtenberg D, Andelman D. Shape of phospholipid/surfactant mixed micelles: cylinders or disks? Theoretical analysis. J Phys Chem B 1997;101:6600–6.
[36] Bergström LM, Skoglund S, Danerlöv K, Garamus VM, Pedersen JS. The growth of micelles, and the transition to bilayers, in mixtures of a single-chain and a double-chain cationic surfactant investigated with small-angle neutron scattering. Soft Matter 2011;7:10935–44.
[37] Granek R, Gelbart WM, Bohbot Y, Ben-Shaul A. Smectic-A to bilayer evolution in concentrated surfactant solutions: the role of spontaneous curvature. J Chem Phys 1994;101:4331–42.
[38] Cuesta JA, Sear RP. Phase transitions in simple models of rod-like and disc-like micelles. Eur Phys J B 1999;8:233–43.
[39] Gelbart WM, Ben-Shaul A. The "new" science of "complex fluids". J Phys Chem 1996;100:13169–89.
[40] Israelachvili JN, Mitchell DJ, Ninham BW. Theory of self-assembly of hydrocarbon amphiphiles into micelles and bilayers. J Chem Soc Faraday Trans I 1976;72:1525–68.
[41] Israelachvili JN. Intermolecular and surface forces. 3rd ed. London: Academic Press; 2011.
[42] Alargova RG, Danov KD, Kralchevsky PA, Broze G, Mehreteab A. Growth of giant rodlike micelles of ionic surfactant in the presence of Al^{3+} counterions. Langmuir 1998;14:4036–49.
[43] Sorensen CM, Shi D. Guinier analysis for homogeneous dielectric spheres of arbitrary size. Opt Commun 2000;178:31–6.
[44] Berne BJ, Pecora R. Dynamic light scattering. New York: Wiley; 2000.
[45] Van de Sande W, Persoons A. The size and shape of macromolecular structures: determination of the radius, the length, and the persistence length of rodlike micelles of dodecyldimethylammonium chloride and bromide. J Phys Chem 1985;89:404–6.
[46] Alargova RG, Ivanova VP, Kralchevsky PA, Mehreteab A, Broze G. Growth of rod-like micelles in anionic surfactant solutions in the presence of Ca^{2+} counterions. Colloids Surf A 1998;142:201–18.
[47] Leaver MS, Holmes MC. A small angle neutron scattering study of the lamellar and nematic phases of caesium pentadecafluoro-octanoate (CsPFO)/^2H_2O and CsPFO/CsCl/^2H_2O. J Phys II Fr 1993;3:105–20.
[48] Scheraga HA. Non-Newtonian viscosity of solutions of ellipsoidal particles. J Chem Phys 1955;23:1526–32.